Journal of Applied Physics

Enhanced optical mode coherence in exchange coupled soft magnetic multilayers

Cite as: J. Appl. Phys. **131**, 213902 (2022); https://doi.org/10.1063/5.0093827
Submitted: 30 March 2022 • Accepted: 13 May 2022 • Published Online: 02 June 2022

H. Liu, Agne Ciuciulkaite, Vassilios Kapaklis, et al.

J. Appl. Phys. **131**, 213902 (2022); https://doi.org/10.1063/5.0093827 **131**, 213902

AIP Publishing

Enhanced optical mode coherence in exchange coupled soft magnetic multilayers

Cite as: J. Appl. Phys. **131**, 213902 (2022); doi: 10.1063/5.0093827
Submitted: 30 March 2022 · Accepted: 13 May 2022 ·
Published Online: 2 June 2022

H. Liu,[1] Agne Ciuciulkaite,[2] Vassilios Kapaklis,[2] D. Karaiskaj,[1,a)] and D. A. Arena[1,b)]

AFFILIATIONS

[1] Department of Physics, University of South Florida, Tampa, Florida 33620, USA
[2] Department of Physics and Astronomy, Uppsala University, Uppsala, Sweden

[a)] **E-mail:** karaiskaj@usf.edu
[b)] **Author to whom correspondence should be addressed:** darena@usf.edu

ABSTRACT

We report on an all-optical investigation of coupled spin excitation modes in a series of magnetic trilayer structures. Using time-resolved magneto-optic Kerr effect (tr-MOKE) magnetometry, we observe multi-mode coherent spin excitations in $\mathrm{Ni_{81}Fe_{19}/Ru/Co_{49}Fe_{49}V_2}$ multilayers even though the tr-MOKE optical detection is sensitive only to the $\mathrm{Co_{49}Fe_{49}V_2}$ magnetization dynamics. Frequency shifts of the different modes indicate that the coupling between the $\mathrm{Ni_{81}Fe_{19}}$ and $\mathrm{Co_{49}Fe_{49}V_2}$ layers varies from anti-ferromagnetic to ferromagnetic to uncoupled as the Ru spacer layer thickness is increased from 8 Å to 200 Å. The lifetime of the high frequency coherent oscillations in the $\mathrm{Co_{49}Fe_{49}V_2}$ layer increases by over 200%–300% even in the case of uncoupled $\mathrm{Ni_{81}Fe_{19}}$ and $\mathrm{Co_{49}Fe_{49}V_2}$ layers with a 200 Å thick Ru spacer. The results suggest an additional method to decrease the damping of high-moment alloys in layered magnetic nanostructures.

INTRODUCTION

Magnetic multilayers are the foundation of advanced spintronic phenomena and technology, including giant magnetoresistance,[1,2] magnetic tunnel junctions,[3–6] and other applications.[7–11] The GHz-scale and higher frequency excitation modes of such multilayer structures are of paramount importance in diverse applications, such as magnetic field sensors,[12] spin-torque oscillators,[13–17] and magnonic circuit elements.[18] For such applications, resonance modes with large amplitude and long spin coherence lifetimes are desirable.

The collective resonance modes of magnetic trilayers, where two magnetic layers (A and B) are separated by a non-magnetic (NM) layer, offer additional approaches to modify the resonance characteristics, particularly as material selection and the thickness of the NM layer can alter the coupling between the two magnetic layers.[19,20] When the interlayer exchange coupling (IEC) is ferromagnetic, the collective resonance modes of the trilayer are the low energy acoustic mode and the higher energy optical mode.[21–23] In the acoustic mode, the magnetization of the two layers is excited into an oscillatory precession orbits with identical amplitude and phase. The resonant frequency of the mode is governed by the standard ferromagnetic resonance (FMR) mode: $\omega_{(A,B)} = \gamma_{(A,B)}\,\mu_0\sqrt{H\big(H + M_{eff,(A,B)}\big)}$, where γ is the gyromagnetic ratio, M_{eff} is the effective magnetization (including volume magnetization, anisotropy, and dipolar fields), and $\mu_0 H$ is the applied external field. For the optical mode excitation, the magnetization precesses out of phase, changing the angle between the magnetization of the layers throughout the precession orbit, leading to an additional energy contribution and, hence, a higher precession frequency. However, for identical magnetic layers, the contributions of the layers cancel throughout the precession orbit, leading to a mode with vanishing intensity.[24,25]

Quasi-optical modes in asymmetric trilayers, where $M_{eff,A} \neq M_{eff,B}$, can exhibit an appreciable intensity as the resonant response of the individual layers do not cancel completely. In asymmetric trilayers, the quasi-acoustic and quasi-optic modes, which we refer to as optical and acoustic modes for simplicity, have their resonant modes modified by the interlayer exchange coupling constant J_{AB},

$$\begin{aligned} \omega_{ac}^2 &= \omega_B^2 + J_{AB}\,\frac{\gamma_B^2\cos(\theta_A-\theta_B)\,\cdot\,\big(2\mu_0 H_{app}\big)}{d_B\,M_{eff,B}},\\ \omega_{op}^2 &= \omega_A^2 + J_{AB}\,\frac{\gamma_A^2\cos(\theta_A-\theta_B)\,\cdot\,\big(2\mu_0 H_{app}\big)}{d_A\,M_{eff,A}}, \end{aligned} \tag{1}$$

where we assume that $M_{eff,B} < M_{eff,A}$ and we assume negligible anisotropy in the samples.[26] ω_{ac} (ω_{op}) is the frequency of the acoustic (optical) mode, ω_A (ω_B) is the single layer FMR frequency for layer A (B), γ_A (γ_B) is the gyromagnetic ratio for A (B), d_A (d_B) is the layer thickness, and θ_A (θ_B) is the equilibrium angle of the magnetization. H_{app} is the applied field, and in our geometry [Fig. 1(a)], this term dominates over the demagnetization energy. In this formulation, J_{AB} is expressed as energy per unit area.

Our samples consist of two magnetic layers separated by a non-magnetic coupling layer. We use the high-moment $Co_{49}Fe_{49}V_2$ alloy (Permendur or Pmd) and the lower moment but also lower damping $Ni_{81}Fe_{19}$ (Permalloy or Py) for the magnetic layers. Ru is used for the coupling layer as it enables strong IEC that oscillates from ferromagnetic $J_{AB} > 0$ to anti-ferromagnetic $J_{AB} < 0$ with a decaying amplitude as a function of Ru thickness.[20] In Fig. 1(b), we calculate the effects of J_{AB} on the resonant modes of the structure. The solid lines (red for Pmd, blue for Py) depict the frequency vs applied field relation for uncoupled layers (that is, $J_{AB} = 0$) for our experimental geometry; in the zero coupling case, the dynamics of the layers are independent. When $J_{AB} \neq 0$, the individual resonant modes become coupled, and we refer to the higher (lower) energy response as the optical (acoustic) mode. For FM coupling, Eq. (1) indicates the resonant frequency shifts upward while the opposite occurs for AF coupling and the frequency shift for the Pmd/Ru/Py system is larger for the acoustic mode. In magnetic multilayers, the acoustic and optic modes are often resolved using fixed-frequency FMR, where a single frequency is used to excite precession and the resonant response is monitored as a function of an applied external field. In our measurements, we detect these oscillation modes using the time-resolved magneto-optic Kerr (tr-MOKE) effect with fs-time resolution at a fixed external field.[21,22] This method reveals the interplay between the two resonant modes, which occur at a fixed field but different frequencies.

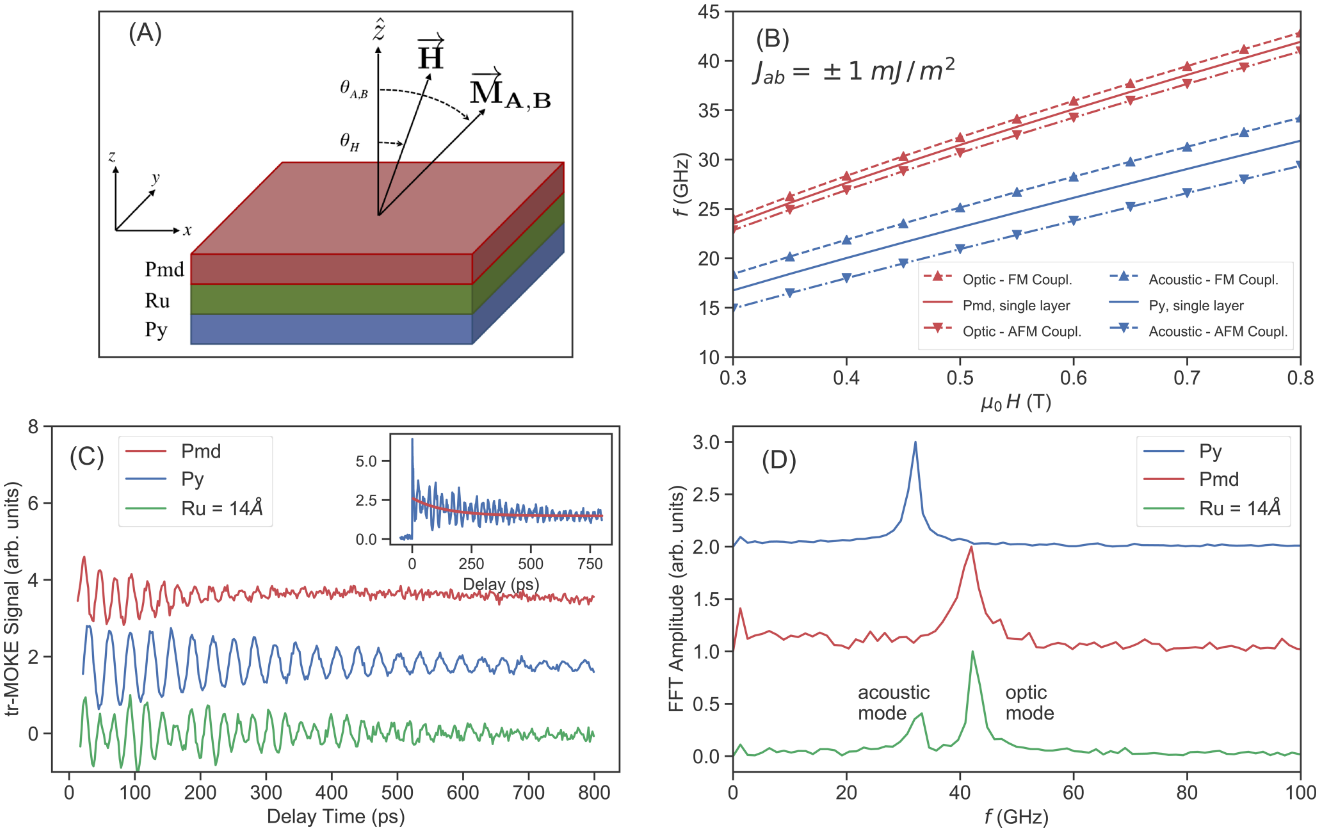

FIG. 1. (a) Coordinate system. The applied field $\vec{H}$ lies in the x, z plane and makes an angle θ_H with respect to the z axis. $\vec{M}_{A,B}$ depicts the magnetization of layer A (Pmd) or B (Py). (b) Evolution of single layer resonance curves into collective quasi-optical and quasi-acoustic excitations. The Pmd (red) and Py (blue) single layer oscillations are coupled by the exchange interaction J_{AB}. The quasi-optical mode (red) shifts to higher (lower) frequency from the Pmd single layer resonance for $J_{AB} > 0$ ($J_{AB} < 0$) indicating FM (AFM) coupling. (c) FMR oscillations at $\mu_0 H = 0.6$ T in the tr-MOKE signal for single layer Pmd and Py, and a Pmd/Ru 14 Å/Py trilayer. In the main panel, the tr-MOKE signal from the $d_{Ru} = 14$ Å trilayer sample exhibits a beating pattern indicating an oscillation mode with multiple frequencies. Inset: the full tr-MOKE signal (blue) and exponential decay (red). Following the initial ultrafast demagnetization, the FMR oscillations are superimposed on the exponential background. (d) Fast Fourier Transform of the time delay data in panel (c). The $d_{Ru} = 14$ Å trilayer sample (green) shows the bi-modal frequency distribution for coupled layers.

SAMPLES AND METHODS

The thin film magnetic multilayers were prepared using room temperature DC magnetron sputtering onto oxidized Si substrates. The structure of the samples is: substrate/Ta [30 Å]/Py [80 Å]/Ru [d_{Ru}]/Pmd [80 Å]/Ta [30 Å]. The Ru spacer layer thickness (d_{Ru}) was varied between 8 Å up to 200 Å to modify the IEC from favoring anti-parallel ($d_{Ru} = 8$ Å and 11 Å) and parallel ($d_{Ru} = 14$ Å) ground state coupling; the thickest sample measured ($d_{Ru} = 200$ Å) is expected to have negligible coupling. Samples consisting of single magnetic layers (Pmd or Py) with the same seed and cap layers were also grown. Static magnetic properties are measured with both a vibrating sample magnetometer (VSM) and static MOKE in an in-plane configuration $\theta_H = 90^\circ$. Static MOKE scans acquired at the tr-MOKE measurement angle of $\theta_H = 70^\circ$ indicate that all samples are at or very close to saturation for an applied field of $\mu_0 H \geq 0.3$ T.

Figure 1(a) presents the geometry of our tr-MOKE measurements; for clarity, in the figure, the seed and cap layers are omitted. The thin film samples are aligned along the x, y-plane with $\hat{z}$ as the surface normal. The variable external magnetic field $\mathbf{H}$ is applied at an angle $\theta_H = 70^\circ$ with respect to $\hat{z}$ and we define the equilibrium polar angle of the magnetization of the layers ($\mathbf{M_{A,B}}$) by $\theta_{A,B}$ ($A = $ Pmd and $B = $ Py). In our measurements, the applied field strength $\mu_0 H$ varies between 0.3 and 0.8 T and, hence, the magnetization is nearly in-plane. Even at the highest applied field, we estimate that the static equilibrium angle θ_A (θ_B) is 86° (88°), where 90° is in-plane, and that the contribution to the total energy from demagnetization is less than 10%. Following the ultrafast pump pulse, the system rapidly demagnetizes, reducing $|\vec{M}_A|$ and $|\vec{M}_B|$ and also modifying the anisotropy; the reduction of both the magnetization and anisotropy establishes a new equilibrium angle (θ'_A or θ'_B). After ~10 ps, the system cools sufficiently to reestablish the magnitude of the magnetization, which now points along the modified angles θ'_A and θ'_B, leading to precession of the magnetization of the different layers about their original equilibrium angles θ_A and θ_B.[27]

The tr-MOKE apparatus consists of a pulsed Ti-sapphire regenerative amplifier with a central wavelength of 800 nm and a pulse duration of 100 fs. The linearly polarized 800 nm light was split into pump and probe beams and the pump beam was frequency doubled to 400 nm to facilitate unique detection of the probe. The pump and probe fluences were measured to be ~0.4 and ~0.075 mJ/cm^2, respectively, and the pump beam is ~ 3× the size of the probe. The beams overlap on the sample at near-normal incidence. The Kerr rotation was measured by passing the reflected probe beam through a $\lambda/2$ plate and then onto a Wollaston prism, which directed the s and p components of the polarization onto a balanced Si photodetector. Timing scans were generated with a mechanical stage that varies the time delay between the 400 nm pump and 800 nm probe beams.

Figure 1(c) displays tr-MOKE delay scans for the single layer Pmd (red), Py (blue) and a trilayer with $d_{Ru} = 14$ Å (green) for $\mu_0 H = 0.6$ T. The inset to the figure displays the full tr-MOKE time delay scan in blue. At a delay $t_D = 0$ ps, the ultrafast demagnetization process is apparent in the sharp rise of the tr-MOKE signal. The magneto-optical response at larger values of t_D is characterized by rapid oscillations superimposed upon an exponential return to the pre-pump equilibrium value. To generate the timing scans in the main panel of Fig. 1(c), we restrict the data to $t_D > 10$ ps and then subtract the exponential background (red) from the raw tr-MOKE signal (blue). The resulting timing scans exhibit exponentially decaying oscillations characterized by one or more frequencies.

Panel (d) presents the fast Fourier transform (FFT) of the data in Fig. 1(c). The magnetization dynamics of the Py and Pmd single layer samples display a single frequency, 26 GHz for Py and 35.8 GHz for Pmd. The Py linewidth is considerably narrower, reflecting the longer decay time (lower damping) of Py; oscillations for Py extend out to at least $t_D = 800$ ps while the higher frequency Pmd oscillations are damped out by ~270 ps. The trilayer sample with $d_{Ru} = 14$ Å (green) exhibits a clear beating pattern characteristic of two oscillation modes, as can be seen in the FFT for the sample in Fig. 1(d). The origin of the mixed mode detected in the magneto-optical response could originate from (1) optical detection of the precession of not only the top metallic layer (Pmd) but also the bottom Py layer and/or (2) excitation of acoustic and optical modes in both layers but detected only from the Pmd layer. The first option can be discounted as the 800 nm probe beam must pass through the Ta cap, Pmd layer, and Ru spacer before reflecting off the Ru/Py interface and then pass through the Ta, Pmd, and Ru layers again prior to detection outside the sample. We estimate that the two way transmission through the layers on top of the Py layer attenuates the 800 nm probe beam by 95% in the case of $d_{Ru} = 8$ Å and essentially 100% for $d_{Ru} = 200$ Å.[28,29] This is a conservative estimate which assumes that the intensity losses of the probe beam arise only from absorption; inclusion of the reflection losses would increase the attenuation of the optical signal from the Py even further. Moreover, neither frequency corresponds to the eigenmodes of single layer samples. Both modes present in the $d_{Ru} = 14$ Å sample are shifted to higher frequencies and the linewidth of the higher frequency mode is considerably narrower than observed in the single layer Pmd sample.

RESULTS AND DISCUSSION

We collected tr-MOKE scans from the samples as a function of applied field $\mu_0 H$ while keeping θ_H fixed at 70°. Results are presented in Fig. 2 for the trilayer samples with varying d_{Ru} (green) as well as the single layer Py (blue) and Pmd (red) reference samples. The precession mode excited in the Py sample has a very long decay time with oscillations clearly detectable out to 800 ps after the pump pulse. At an equivalent field, the Pmd sample displays not only a higher frequency response but also a much shorter decay time.

We model the time-varying component of the Kerr rotation for the Py and Pmd single layers [Fig. 2, panels (e) and (f)] as exponentially damped sinusoidal functions to determine the frequency, decay time and amplitude of the mode: $\theta_K(t) = A\, e^{-t/\tau_D} \sin(\omega t + \phi)$; here, A is the initial amplitude, τ_D is the decay time of the oscillatory mode, ω is the angular frequency of the resonant excitation, and ϕ is an arbitrary phase angle. The resulting fits to the model are shown as blue (Py) and red (Pmd) traces; black traces are the tr-MOKE data. The oscillatory response of the trilayer samples is slightly more complicated as the coupled

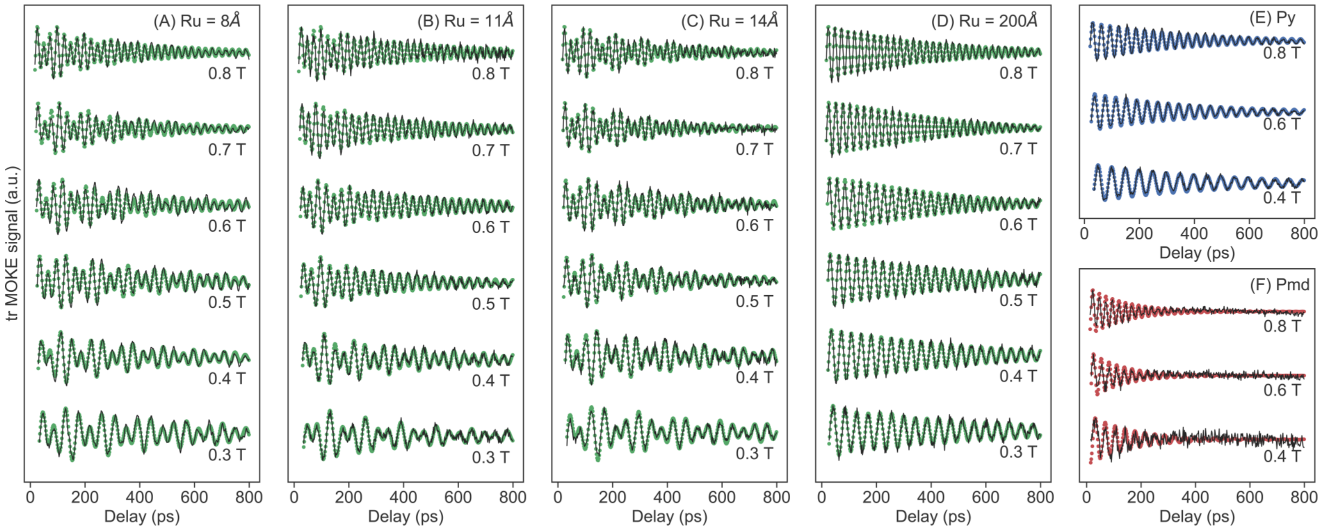

FIG. 2. Representative time delay scans for all samples, offset vertically for clarity. Field values ($\mu_0 H$) are indicated. Panel (a) Ru 8 Å, (b) Ru 11 Å, (c) Ru 14 Å, (d) Ru 200 Å, (e) Py, single layer, (f) Pmd, single layer. tr-MOKE data are the light black traces while the symbols in color (green for tri-layer samples, blue for Py single layer, red for Pmd single layer) are fits to the data using Eq. (2).

layers have two eigenmodes corresponding to the acoustic (*ac*) and optical (*op*) excitations,

$$\theta_K(t) = A_{ac}\, e^{-t/\tau_{D,ac}} \sin(\omega_{ac} t + \phi_{ac}) + A_{op}\, e^{-t/\tau_{D,op}} \sin\left(\omega_{op} t + \phi_{op}\right). \tag{2}$$

Fits for the trilayer samples are also shown in Fig. 2 as green symbols while the light black lines are the data. The fits to the model capture the dynamics in θ_K quite well. We note that we do not observe evidence of a temporal chirp in the data, which is consistent with the low fluences used for the pump and probe beams in our measurement.[30]

Figure 3(a) presents the resonant frequencies of the higher frequency optical (circles) and lower frequency acoustic (squares) modes for the different trilayer samples. The frequencies presented in 3(a) are extracted from Eq. (2); these are very close, but not identical, to the frequencies of peaks in the FFT spectrum of the

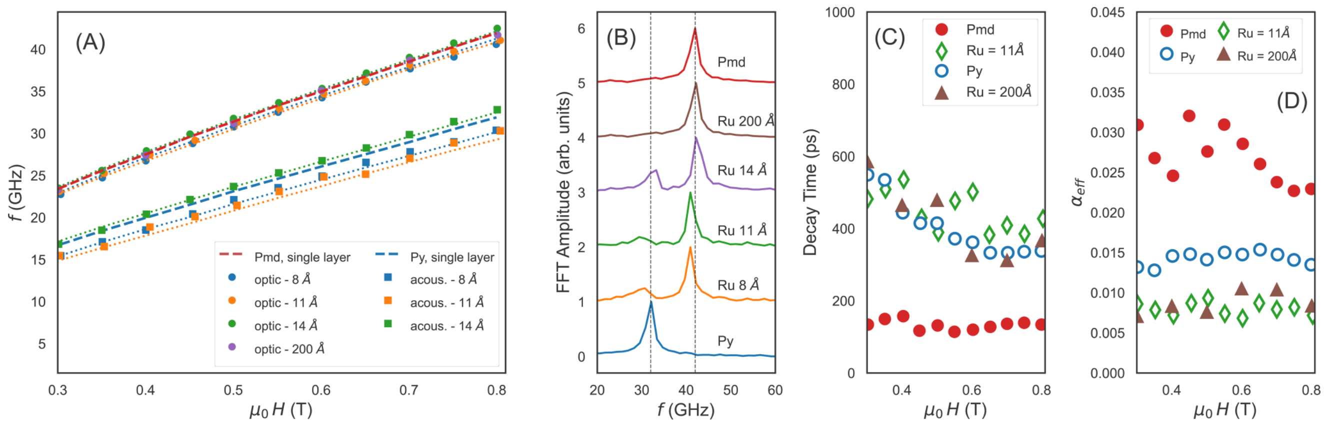

FIG. 3. (a) Resonant fields extracted from the full tr-MOKE data set, along with a fit Eq. (1). Red (Blue) dashed line is for the Pmd (Py) single layer. Shifts to lower (higher) frequency indicate anti-ferromagnetic (ferromagnetic) coupling between the layers. (b) FFT of tr-MOKE data in Fig. 2 at $\mu_0 H = 0.8$ T. The bi-modal response of the trilayer samples with $d_{Ru} = 14$ Å or less can be seen. (c) Decay time ($\tau_{D,op}$) of the high frequency modes, along with τ_D for the single layer Pmd (red filled circle) and Py (open blue circles). Only the $d_{Ru} = 11$ Å and 200 Å trilayer samples are shown; others have a similar response. (d) Damping (α_{eff}) calculated from Eq. (3). The lower damping of the $d_{Ru} = 11$ Å (green diamonds) and $d_{Ru} = 200$ Å (brown triangles) samples relative to the Pmd single layer (red circles) is evident.

time delay data. We also include fits to the single layer Kittel relationship (heavy dashed lines in red and blue for Pmd and Py, respectively) from which we extract the gyromagnetic ratios ($\gamma_A/2\pi = 26.8\,\text{GHz/T}$, $\gamma_B/2\pi = 26.0\,\text{GHz/T}$) and effective magnetization ($\mu_0 M_{eff,A} = 2.24\,\text{T}$, $\mu_0 M_{eff,B} = 1.09\,\text{T}$) for the individual Pmd (A) and Py (B) layers; the saturation magnetization values are within 8% of tabulated values.[31] The high frequency optical mode can be resolved in all four samples with d_{Ru} ranging from 8 Å to 200 Å while the lower frequency acoustic mode is detected only in the $d_{Ru} = 8$, 11, and 14 Å samples. J_{AB} can be estimated from the shifts away from the single layer resonance frequency vs field curves [Eq. (1)]. $J_{AB} = -0.7$ (AF), -1.0 (AF), and $+0.25$ (weak FM) mJ/m^2 for the $d_{Ru} = 8$, 11, and 14 Å samples. Interlayer coupling of similar magnitude has been reported in samples with Ru spacer layers, albeit with different growth order and capping layers.[32]

For the trilayers, both modes are present in all samples except for $d_{Ru} = 200$ Å. In all cases where both modes are present, the optical mode has significantly higher amplitude than the acoustic mode [cf. Fig. 3(b)] and the ratio of the optical to acoustic mode amplitudes is high, ranging from about unity at low fields to ~2 at 0.8 T. Most interestingly, the coherence of the optical mode, as reflected in the decay times of the optical mode [Fig. 3(c)], is enhanced by ~200% or more.

For pure Pmd, the tr-MOKE data in Fig. 2(f) decays rapidly following the initial excitation and the $1/e$ decay time (τ_D) for all fields is ~150 ps [Fig. 3(c), red filled circles]. However, for all the trilayer samples, the precession oscillations corresponding to the high frequency optical mode persist out to 800 ps or longer [Figs. 2(a) through 2(d)]. $\tau_{D,op}$ for a subset of the samples is also displayed in Fig. 3(c) along with the decay of the single layer Py (blue open circles). We also present in Fig. 3(d) an estimate of the effective damping (α_{eff}) for the optical modes and the single layer films derived from the decay times,

$$\alpha_{eff} = \left[\tau_{D,i}\,\gamma_i\left(H_{app} + \frac{M_{s,i}}{2}\right)\right]^{-1}, \tag{3}$$

where the subscript i labels either the layer (in the case of the Py or Pmd single layers) or the collective optical mode. The description of α_{eff} is adapted from Ref. [33], assuming negligible out-of-plane anisotropy, as is the case in our films. Also, for the optical mode, we have made the simplifying assumption that the gyromagnetic ratio and saturation magnetization of Pmd are reasonable approximations of similar parameters for the collective optical mode. The effective damping of the optical mode in the $d_{Ru} = 11$ Å and $d_{Ru} = 200$ Å samples is seen to be largely independent of the applied field and, hence, largely independent of frequency. The data show that the optical mode in the trilayer samples oscillates with a large amplitude, high frequency and long decay time, or equivalently, low damping. The oscillatory Kerr rotation can neither originate from reflection off of the Ru/Py interface nor deeper into the Py layer. Hence, the tr-MOKE signal reflects the magnetization dynamics of the Pmd layer alone.

Several features of the study stand out. First, in trilayer structures where the two magnetic layers are even weakly coupled, following an ultrafast optical excitation the precession modes of the system deviate from that of a single layer and can be considered as a collective response of the system: that is, the optical and acoustic modes. Second, in our system with magnetic layers where the effective magnetization differs by over a factor of 2 (Pmd to Py), weak ferromagnetic coupling increases the frequencies of the optical and acoustic modes, but only by a few GHz; the higher frequency optical mode remains close to the precession mode of a single Pmd layer. However, the most salient aspect of the study is the enhancement of the decay time in the higher frequency optical mode from ~150 ps for pure Pmd to ~400 ps at $f = 40$ GHz and even longer at lower frequencies. Indeed, the effective damping of the optical mode in the trilayer samples is lower than Py, under the assumption that the gyromagnetic ratio and the saturation magnetization of Pmd are appropriate surrogate values for the collective optical mode of the trilayers.

The results indicate that the magnetization dynamics of the Pmd layer may be influenced by the dynamics of the underlying Py layer in our tri-layer structures. While the origin of this effect is not firmly established, we point to a few considerations that may be relevant to the reduced damping in the Pmd layer. The crystallinity and film texture of the Pmd layer may play a role in the dynamic behavior as the single layer Pmd film was grown on a Ta seed while in the trilayer samples, the Pmd layers were grown on top of the Ru spacer. While our Pmd layers had a thickness of only 80 Å, studies of thick (1000 Å) films of the closely related $\text{Fe}_{65}\text{Co}_{35}$ alloy grown on Ta exhibit a considerably larger fixed-frequency FMR linewidth compared to films grown on Ru.[34] However, Ru has a long spin diffusion length[35,36] and spin transport from one magnetic layer through the Ru spacer can influence the dynamics of a second magnetic layer.[37] In similar Py/Ru/Pmd structures studied with fixed-frequency excitations, the non-resonant layer experiences an appreciable precession amplitude when the other layer is driven through its resonance.[38] Also, in the trilayer structures, the top and bottom interfaces of the Pmd are Ta and Ru, respectively, which have opposite spin Hall conductivities.[39,40] The asymmetric nature of the spin-active interfaces may help stabilize the lower damping of Pmd observed in the trilayer structures. Additional factors that may affect the spin dynamics of the layers include chiral magnon pumping,[41] strong magnon–magnon coupling between the layers,[42] spin pumping,[43] and an anti-damping torque due to the spin Hall effect.[44,45]

Regardless of the origin, our results suggest an additional method for modifying the damping in a heterogeneous magnetic structure. As the design of spintronic devices frequently involves optimization of competing materials parameters, for example, achieving high spin polarization or layer magnetization while maintaining acceptably low damping, the ability to considerably reduce the damping in a selected layer by off-resonant excitation of a coupled layer could expand the design options for spintronic field sensors, oscillators, magnetic tunnel junctions, and related devices.

ACKNOWLEDGMENTS

We thank Mojtaba Ranjbar and Johan Åkerman for their assistance in the fabrication of the samples. This material was based upon work supported by the National Science Foundation

(NSF) under Grant No. ECCS-1952957. D.A.A. acknowledges the support of the USF Nexus Initiative and the Swedish Fulbright Commission. V.K. acknowledges financial support from the Swedish Research Council (Project No. 2019-03581) and the Carl Tryggers Foundation (Project No. 19:175).

AUTHOR DECLARATIONS

Conflict of Interest

The authors have no conflicts to disclose.

DATA AVAILABILITY

The data that support the findings of this study are available from the corresponding author upon reasonable request.

REFERENCES

[1] M. N. Baibich, J. M. Broto, A. Fert, F. N. Van Dau, and F. Petroff, "Giant magnetoresistance of (001)Fe/(001)Cr magnetic superlattices," Phys. Rev. Lett. **61**, 2472–2475 (1988).

[2] G. Binasch, P. Grünberg, F. Saurenbach, W. Zinn, P. Grunberg, F. Saurenbach, and W. Zinn, "Enhanced magnetoresistance in layered magnetic structures with antiferromagnetic interlayer exchange," Phys. Rev. B **39**, 4828–4830 (1989).

[3] S. Tehrani, J. M. Slaughter, M. Deherrera, B. N. Engel, N. D. Rizzo, J. Salter, M. Durlam, R. W. Dave, J. Janesky, B. Butcher, K. Smith, and G. Grynkewich, "Magnetoresistive random access memory using magnetic tunnel junctions," Proc. IEEE **91**(5), 703–714 (2003).

[4] L. Lagae, R. Wirix-Speetjens, W. Eyckmans, S. Borghs, and J. De Boeck, "Increased Gilbert damping in spin valves and magnetic tunnel junctions," J. Magn. Magn. Mater. **286**, 291–296 (2005).

[5] A. T. Hindmarch, V. Harnchana, E. Negusse, D. A. Arena, A. P. Brown, R. M. D. Brydson, C. H. Marrows *et al.*, "Magnetostructural influences of thin Mg insert layers in crystalline CoFe (B)/MgO/CoFe (B) magnetic tunnel junctions," Appl. Phys. Lett. **97**, 252502 (2010).

[6] K. J. Dempsey, A. T. Hindmarch, H. X. Wei, Q. H. Qin, Z. C. Wen, W. X. Wang, G. Vallejo-Fernandez, D. A. Arena, X. F. Han, and C. H. Marrows, "Cotunneling enhancement of magnetoresistance in double magnetic tunnel junctions with embedded superparamagnetic NiFe nanoparticles," Phys. Rev. B **82**(21), 214415 (2010).

[7] Y. Huai, J. Zhang, G. W. Anderson, P. Rana, S. Funada, C.-Y. Hung, M. Zhao, and S. Tran, "Spin-valve heads with synthetic antiferromagnet CoFe/Ru/CoFe/IrMn," J. Appl. Phys. **85**, 5528 (1999).

[8] J. L. Leal and M. H. Kryder, "Spin valves exchange biased by Co/Ru/Co synthetic antiferromagnets," J. Appl. Phys. **83**, 3720 (1998).

[9] H. van den Berg, W. Clemens, G. Gieres, G. Rupp, W. Schelter, and M. Vieth, "GMR sensor scheme with artificial antiferromagnetic subsystem," IEEE Trans. Magn. **32**(5), 4624–4626 (1996).

[10] A. Soumyanarayanan, N. Reyren, A. Fert, and C. Panagopoulos, "Emergent phenomena induced by spin–orbit coupling at surfaces and interfaces," Nature **539**, 509–517 (2016).

[11] W. Li, I. Bykova, S. Zhang, G. Yu, R. Tomasello, M. Carpentieri, Y. Liu, Y. Guang, J. Gräfe, M. Weigand, D. M. Burn, G. van der Laan, T. Hesjedal, Z. Yan, J. Feng, C. Wan, J. Wei, X. Wang, X. Zhang, H. Xu, C. Guo, H. Wei, G. Finocchio, X. Han, and G. Schütz, "Anatomy of skyrmionic textures in magnetic multilayers," Adv. Mater. **31**, 1807683 (2019).

[12] I. McFadyen, E. Fullerton, and M. Carey, "State-of-the-art magnetic hard disk drives," MRS Bull. **31**, 379–383 (2006).

[13] S. Kaka, M. R. Pufall, W. H. Rippard, T. J. Silva, S. E. Russek, and J. A. Katine, "Mutual phase-locking of microwave spin torque nano-oscillators," Nature **437**, 389–392 (2005).

[14] A. M. Deac, A. Fukushima, H. Kubota, H. Maehara, Y. Suzuki, S. Yuasa, Y. Nagamine, K. Tsunekawa, D. D. Djayaprawira, and N. Watanabe, "Bias-driven high-power microwave emission from MgO-based tunnel magnetoresistance devices," Nat. Phys. **4**, 803–809 (2008).

[15] P. M. Braganca, B. A. Gurney, B. A. Wilson, J. A. Katine, S. Maat, and J. R. Childress, "Nanoscale magnetic field detection using a spin torque oscillator," Nanotechnology **21**, 235202 (2010).

[16] N. Locatelli, V. Cros, and J. Grollier, "Spin-torque building blocks," Nat. Mater. **13**, 11–20 (2014).

[17] E. Jué, W. H. Rippard, and M. R. Pufall, "Comparison of the spin-transfer torque mechanisms in a three-terminal spin-torque oscillator," J. Appl. Phys. **124**, 043904 (2018).

[18] K. Szulc, S. Mendisch, M. Mruczkiewicz, F. Casoli, M. Becherer, and G. Gubbiotti, "Nonreciprocal spin-wave dynamics in Pt/Co/W/Co/Pt multilayers," Phys. Rev. B **103**, 134404 (2021).

[19] S. Parkin, N. More, and K. Roche, "Oscillations in exchange coupling and magnetoresistance in metallic superlattice structures: Co/Ru, Co/Cr, and Fe/Cr," Phys. Rev. Lett. **64**, 2304–2307 (1990).

[20] S. Parkin, "Systematic variation of the strength and oscillation period of indirect magnetic exchange coupling through the 3d, 4d, and 5d transition metals," Phys. Rev. Lett. **67**, 3598–3601 (1991).

[21] A. Barman, V. V. Kruglyak, R. J. Hicken, C. H. Marrows, M. Ali, A. T. Hindmarch, and B. J. Hickey, "Characterization of spin valves fabricated on opaque substrates by optical ferromagnetic resonance," Appl. Phys. Lett. **81**, 1468–1470 (2002).

[22] R. J. Hicken, A. Barman, V. V. Kruglyak, and S. Ladak, "Optical ferromagnetic resonance studies of thin film magnetic structures," J. Phys. D: Appl. Phys. **36**, 2183–2192 (2003).

[23] C. Berk, F. Ganss, M. Jaris, M. Albrecht, and H. Schmidt, "All-optical measurement of interlayer exchange coupling in Fe/Pt/FePt thin films," Appl. Phys. Lett. **112**, 052401 (2018).

[24] Z. Zhang, L. Zhou, P. Wigen, and K. Ounadjela, "Using ferromagnetic resonance as a sensitive method to study temperature dependence of interlayer exchange coupling," Phys. Rev. Lett. **73**, 336–339 (1994).

[25] J. Lindner and K. Baberschke, "Ferromagnetic resonance in coupled ultrathin films," J. Phys.: Condens. Matter **15**, S465–S478 (2003).

[26] For a derivation, please refer to Eq. (7) in Ref. 46 ufnder the simplifying assumption of negligible anisotropy.

[27] M. van Kampen, C. Jozsa, J. T. Kohlhepp, P. LeClair, L. Lagae, W. J. M. de Jonge, and B. Koopmans, "All-optical probe of coherent spin waves," Phys. Rev. Lett. **88**, 227201 (2002).

[28] W. S. Werner, K. Glantschnig, and C. Ambrosch-Draxl, "Optical constants and inelastic electron-scattering data for 17 elemental metals," J. Phys. Chem. Ref. Data **38**(4), 1013–1092 (2009).

[29] K. K. Tikuišis, L. Beran, P. Cejpek, K. Uhlírová, J. Hamrle, M. Vanatka, M. Urbánek, and M. Veis, "Optical and magneto-optical properties of permalloy thin films in 0.7–6.4 eV photon energy range," Mater. Des. **114**, 31–39 (2017).

[30] S. Mondal and A. Barman, "Laser controlled spin dynamics of ferromagnetic thin film from femtosecond to nanosecond timescale," Phys. Rev. Appl. **10**, 054037 (2018).

[31] J. Coey, *Magnetism and Magnetic Materials* (Cambridge University Press, Cambridge, 2010).

[32] Y. Wei, S. Jana, R. Brucas, Y. Pogoryelov, M. Ranjbar, R. K. Dumas, P. Warnicke, J. Akerman, D. A. Arena, O. Karis, and P. Svedlindh, "Magnetic coupling in asymmetric FeCoV/Ru/FeNi trilayers," J. Appl. Phys. **115**(17), 17D129 (2014).

[33] J. Walowski, M. D. Kaufmann, B. Lenk, C. Hamann, J. McCord, and M. Münzenberg, "Intrinsic and non-local Gilbert damping in polycrystalline nickel studied by Ti: sapphire laser fs spectroscopy," J. Phys. D: Appl. Phys. **41**, 164016 (2008).

[34] L. Lu, J. Young, M. Wu, C. Mathieu, M. Hadley, P. Krivosik, and N. Mo, "Tuning of magnetization relaxation in ferromagnetic thin films through seed layers," Appl. Phys. Lett. **100**, 022403 (2012).

[35] S. Yakata, Y. Ando, T. Miyazaki, and S. Mizukami, "Temperature dependences of spin-diffusion lengths of Cu and Ru layers," Jpn. J. Appl. Phys. **45**, 3892–3895 (2006).

[36] N. Behera, M. S. Singh, S. Chaudhary, D. K. Pandya, and P. K. Muduli, "Effect of Ru thickness on spin pumping in Ru/Py bilayer," J. Appl. Phys. **117**, 17A714 (2015).

[37] B. Khodadadi, J. B. Mohammadi, J. M. Jones, A. Srivastava, C. Mewes, T. Mewes, and C. Kaiser, "Interlayer exchange coupling in asymmetric Co-Fe/Ru/Co-Fe trilayers investigated with broadband temperature-dependent ferromagnetic resonance," Phys. Rev. Appl. **8**, 014024 (2017).

[38] Y. Pogoryelov, M. Pereiro, S. Jana, A. Kumar, S. Akansel, M. Ranjbar, D. Thonig, D. Primetzhofer, P. Svedlindh, J. Åkerman, O. Eriksson, O. Karis, and D. Arena, "Nonreciprocal spin pumping damping in asymmetric magnetic trilayers," Phys. Rev. B **101**(5), 054401 (2020).

[39] A. Hoffmann, "Spin Hall effects in metals," IEEE Trans. Magn. **49**, 5172–5193 (2013).

[40] J. Sinova, S. O. Valenzuela, J. Wunderlich, C. H. Back, and T. Jungwirth, "Spin Hall effects," Rev. Mod. Phys. **87**, 1213 (2015).

[41] H. Wang, M. Madami, J. Chen, L. Sheng, M. Zhao, Y. Zhang, W. He, C. Guo, H. Jia, S. Liu, Q. Song, X. Han, D. Yu, G. Gubbiotti, and H. Yu, "Tunable damping in magnetic nanowires induced by chiral pumping of spin waves," ACS Nano **15**(5), 9076–9083 (2021).

[42] J. Chen, C. Liu, T. Liu, Y. Xiao, K. Xia, G. E. Bauer, M. Wu, and H. Yu, "Strong interlayer magnon-magnon coupling in magnetic metal-insulator hybrid nanostructures," Phys. Rev. Lett. **120**, 217202 (2018).

[43] S. N. Panda, S. Mondal, J. Sinha, S. Choudhury, and A. Barman, "All-optical detection of interfacial spin transparency from spin pumping in b-Ta/CoFeB thin films," Sci. Adv. **5**(4), eaav7200 (2019).

[44] A. Ganguly, R. M. Rowan-Robinson, A. Haldar, S. Jaiswal, J. Sinha, A. T. Hindmarch, D. A. Atkinson, and A. Barman, "Time-domain detection of current controlled magnetization damping in $\mathrm{Pt/Ni_{81}Fe_{19}}$ bilayer and determination of Pt spin Hall angle," Appl. Phys. Lett. **105**, 112409 (2014).

[45] S. Mondal, S. Choudhury, N. Jha, A. Ganguly, J. Sinha, and A. Barman, "All-optical detection of the spin Hall angle in W/CoFeB/$\mathrm{SiO_2}$ heterostructures with varying thickness of the tungsten layer," Phys. Rev. B **96**, 054414 (2017).

[46] G. Wu, W. Zhu, Z. Zhu, H. Xue, Y. Ren, Y. Liu, Q. Y. Jin, and Z. Zhang, "Magnetic precession modes with enhanced frequency and intensity in hard/NM/soft perpendicular magnetic films," Phys. Chem. Chem. Phys. **21**, 16830–16837 (2019).